EPJ manuscript No.
(will be inserted by the editor)

Prospects for Neutron Star Equation of State Constraints using "Recycled" Millisecond Pulsars

Slavko Bogdanov[1]

Columbia Astrophysics Laboratory, Columbia University, 550 West 120th Street, New York, NY 10027, USA

arXiv:1510.06371v1 [astro-ph.HE] 21 Oct 2015

Received: date / Revised version: date

Abstract. "Recycled" millisecond pulsars are a variety of rapidly-spinning neutron stars that typically show thermal X-ray radiation due to the heated surface of their magnetic polar caps. Detailed numerical modeling of the rotation-induced thermal X-ray pulsations observed from recycled millisecond pulsars, including all relevant relativistic and stellar atmospheric effects, has been identified as a promising approach towards an astrophysical determination of the true neutron star mass-radius relation, and by extension the state of cold matter at densities exceeding those of atomic nuclei. Herein, I review the basic model and methodology commonly used to extract information regarding neutron star structure from the pulsed X-ray radiation observed from millisecond pulsars. I also summarize the results of past X-ray observations of these objects and the prospects for precision neutron star mass-radius measurements with the upcoming Neutron Star Interior Composition Explorer (NICER) X-ray timing mission.

PACS. 04 General relativity and gravitation – 20 Nuclear Physics

1 Introduction

The state of cold matter at densities exceeding those of atomic nuclei remains one of the principal outstanding problems in modern physics. Neutron stars provide the only known setting in the Universe where these physical conditions occur naturally. Thermal X-ray radiation from the physical surface of a neutron star can serve as a powerful tool for probing the poorly understood behavior of the matter in the ultra-dense stellar interior (see, e.g., [29] for a comprehensive review). This is possible because of the unique mapping between the pressure and density of neutron star matter and the stellar radius and mass. For neutron stars with thermal radiation confined to a small fraction of the surface, realistic modeling of the rotation-induced flux variations of the observed "hot spot" radiation can, in principle, yield the true $M-R$ relation [35] [11] [10]. Such emission geometry is observed in several varieties of neutron stars including rotation-powered "recycled" millisecond pulsars (MSPs). Recycled MSPs are a population of old neutron stars, characterized by rapid rotation rates (hundreds of Hertz), exceptional rotational stability and low magnetic fields ($\sim 10^{8-9}$ G). It is commonly accepted that these neutron stars are a product of low-mass X-ray binaries [1], acquiring their rapid spin rates via accretion of matter and angular momentum. At the end of their spin-up phase, they are reactivated (i.e., "recycled") as rotation-powered, radio-loud pulsars, meaning that the observer radiation is generated at the expense of the rotational kinetic energy of the neutron star.

Over the past ∼15 years, extensive studies with *Chandra* and *XMM-Newton* have shown that many of these neutron stars are seen as X-ray sources due to their hot ($\sim 10^6$ K) polar caps [52] [9] [12] [18]. The inferred emitting areas indicate that this radiation is localized in regions on the stellar surface that are much smaller than the total surface area, but comparable in radius to what is expected for pulsar magnetic polar caps, $R_{pc} = (2\pi R/cP)^{1/2}$, where R is the stellar radius and P its spin period. This finding is consistent with pulsar electrodynamics models, which predict heating of the polar caps by a backflow of energetic particles along the open magnetic field lines [23]. Sophisticated modeling of the X-ray spectra and pulse profiles (i.e. waveforms) of MSPs can offer a probe of the mass and radius of the star. This approach, originally proposed by [35] in the context of "recycled" MSPs, can serve as a valuable probe of key NS properties that are inaccessible by other observational means.

Below, I provide an overview of the standard approach used for modeling the surface emission from neutron stars in general, and rapidly spinning objects such as MSPs, in particular. I summarize the application of this method in practice to existing data obtained with *XMM-Newton*. I conclude by describing the forthcoming Neutron Star Interior Composition Explorer X-ray timing mission and the precise measurement of neutron star structure it is expected to achieve.

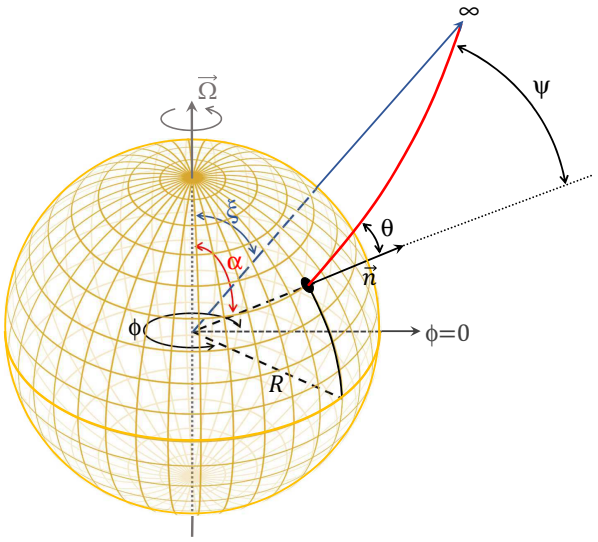

Fig. 1. The geometry of a hot spot on the surface of a rotating neutron star. A non-radial photon emitted from the surface at an angle θ with respect to the local surface normal n is observed at infinity at an angle ψ due to gravitational bending of light. The time-dependent position of the hot spot relative to the observer and the neutron star spin angular momentum vector is uniquely defined by the three angles α, ζ and ϕ through equation (1).

2 Modeling the Surface Emission from Neutron Stars

Conceptually, modeling the thermal radiation from a small region on a slowly-spinning neutron star is fairly straightforward. The observational characteristics of such a hot spot on a compact object were first worked out by Pechenick, Ftaclas, and Cohen [36] and variations and improvements of their formalism have subsequently been presented in a number of other works [19] [13] [43] [30] [13] [5] [38] [51].

2.1 System Geometry and Relativistic Effects

In its simplest form, a model of a neutron star consists of a rotating compact star of mass M, radius R, spin period P, and a single small (point-like) hot spot, though it can be easily generalized to include an arbitrary distribution of emitting surface elements. The hot spot is separated by an angle α from the rotation axis of the star, which in turn is oriented at an angle ζ relative to the line of sight to a distant observer (see the schematic illustration in Figure 1). The position of a hot spot on the stellar surface is defined by ψ, the angle between the normal to the surface and the observer's line of sight:

$$\cos\psi(t) = \sin\alpha\sin\zeta\cos\phi(t) + \cos\alpha\cos\zeta \qquad (1)$$

The time-dependent angle $\phi(t)$ corresponds to the rotational phase of the pulsar, with $\phi = 0$ typically defined to be the time of closest approach of the hot spot to the observer.

In the vicinity of a neutron star, gravity greatly affects the photons as they propagate from the surface to a distant observed. For many practical purposes, the commonly used spherical Schwarzschild + Doppler formalism provides a sufficiently accurate description of the space-time near the stellar surface. It should be noted, however, that for objects spinning at rates greater than ∼300 Hz, the rapid rotation results in appreciable oblateness of the neutron star although the external space-time is still well represented by the Schwarzschild metric [14] [31]. In such instances it is necessary to consider an oblate spheroid. For MSPs with spin frequencies up to ∼800 Hz, the effect on the stellar oblateness on the observed hot spot flux modulations can be as high as 5–30%, while the effect on the space-time quadrupole is 1-5% [40]. In this regime, the Hartle-Thorne metric [24] provides an accurate approximation of the space-time [3]. For the fastest spinning neutron stars (beyond ∼1000 Hz), higher order space-time multipoles are non-negligible, which necessitates numerically solving the field equations for a given neutron star equation of state [15] [47].

As a photon climbs out of the deep gravitational potential, its energy is diminished by $1 + z_g = (1 - R_S/R)^{-1/2}$, where $R_S = 2GM/c^2$, Additionaly, the trajectory of a photon emitted at an angle $\theta > 0$ relative to the local radial direction is deflected, resulting in an angle $\psi > \theta$ measured at infinity. In Schwarzschild geometry, the relation between these two quantities is expressed by the elliptical integral [36]:

$$\psi = \int_R^\infty \frac{\mathrm{d}r}{r^2}\left[\frac{1}{b^2} - \frac{1}{r^2}\left(1 - \frac{R_S}{r}\right)\right]^{-1/2} \qquad (2)$$

where

$$b = \frac{R}{\sqrt{1 - R_S/R}}\sin\theta \qquad (3)$$

is the impact parameter of a light ray originating from radius R (at the neutron star surface) that is emitted at an angle θ. As the use of the ray-tracing integral is computationally demanding, for many applications it is more convenent to use the greatly simplified approximate formula [5] [37]

$$\cos\psi \approx \frac{\cos\theta - R_S/R}{1 - R_S/R} \qquad (4)$$

which can be used for $R > 2R_S$, where it achieves fractional errors of only a few percent at the largest values of θ. However, if high accuracy is desired, the exact expression needs to be used. Due to the deflection of the photon paths by the immense gravitational field, a larger fraction of the stellar surface is visible to an observer at any instance. In the weak-field regime, the visibility condition is simply $\cos\psi = \cos\theta > 0$. In contrast, in the presence of strong gravity regions on the far side of the neutron star relative to the observer surface are viewable up to an angle $\cos\psi_c$, corresponding to the maximum impact parameter $b_{\max} = R/\sqrt{1 - R_S/R} \equiv R^\infty$, the so-called radius at infinity.

For MSPs, the rapid motion of the neutron star surface induces a substantial Doppler effect, parameterized

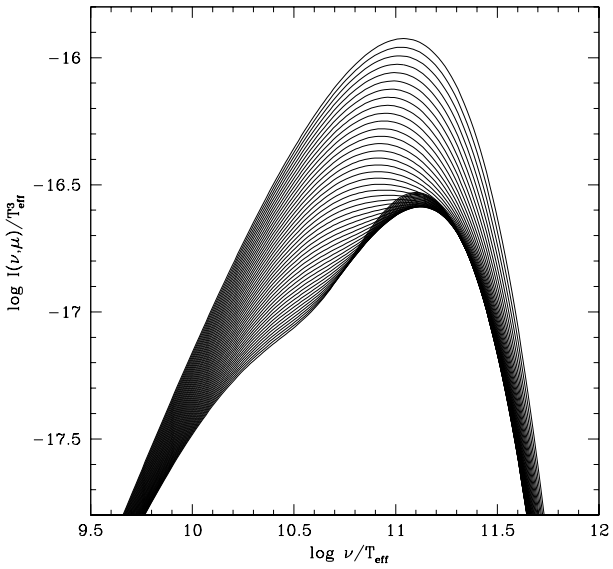

Fig. 2. The emergent intensity of a non-magnetic neutron star hydrogen atmosphere with an effective temperature of 2.1×10^6 Kelvin and a surface gravity of 2.4×10^{14} cm s^{-2} (corresponding to a neutron star with mass 1.4 $M_\odot$ and intrinsic radius 12 km). The different spectra correspond to increasing emission angle with respect to the surface normal (from top to bottom, respectively) in logarithmic steps of 0.3 in $\cos\theta$. Note the shift in the peak of the spectrum towards lower energies in with increasing angle, in addition to the overall decline in intensity. This energy-dependent limb-darkening effect arises due to an temperature gradient within the atmosphere with temperature decreasing towards the surface combined with the fact that at larger viewing angles the observer sees less deep into the atmosphere.

through the familiar Doppler factor

$$\eta = \frac{1}{\gamma(1 - v/c\cos\xi)} \tag{5}$$

where $\gamma = 1/\sqrt{1-(v/c)^2}$, $v = 2\pi R/P(1-R_S/R)^{-1/2}\sin\alpha$ is the velocity of the emitting region as measured in the inertial frame of the neutron star surface, and ξ is the angle between the directions of the velocity vector and towards the observer. This angle can be cast as a function of θ, ψ, ζ, and ϕ [38] [51] as

$$\cos\xi = -\frac{\sin\theta}{\sin\psi}\sin\zeta\sin\phi \tag{6}$$

A simplified approximate expression can be obtained by substituting $\sin\theta/\sin\psi$ with $(1-R_S/R)^{1/2}$, its asymptotic value for small angles.

Photons emitted from the back side of the compact object as seen by the observer, in addition to following a curved trajectory, have to travel an additional distance compared to a photon emitted radially from the near side. The time lag of the photon as recorded by an observer at infinity is given by the elliptical integral [36]

$$\Delta t(b) = \frac{1}{c}\int_R^\infty \frac{\mathrm{d}r}{1-R_S/R}\left\{\left[1-\frac{b^2}{r^2}\left(1-\frac{R_S}{r}\right)\right]^{-1/2} - 1\right\} \tag{7}$$

This time delay translates into a phase lag ($\Delta\phi$) of a photon

$$\Delta\phi = \frac{2\pi}{P}\Delta t \tag{8}$$

which produces the measured rotational phase $\phi_{\rm obs} = \phi + \Delta\phi$ [51]. For $R/R_S = 2.5$, the largest value of Δt, obtained for light rays with maximum impact parameter $b_{\rm max} = (1+z_g)R$, is ≈60 μs. These propagation time differences amount to a few percent of the rotation period of a typical MSP so they need to be taken into account when considering high-quality data.

The flux per unit frequency from a hot spot on a neutron star measured by a distant observed can be expressed as

$$F(\nu) = I(\nu)\mathrm{d}\Omega \tag{9}$$

where $I(\nu)$ is the intensity of the radiation as measured at infinity and $\mathrm{d}\Omega$ is the apparent solid angle subtended by the hot spot on the sky. Transforming both quantities to the rest frame of the hot spot yields

$$F(\nu) = (1-R_S/R)^{1/2}\eta^3 I'(\nu',\theta')\cos\theta'\frac{\mathrm{d}\cos\theta}{\mathrm{d}\cos\psi}\frac{\mathrm{d}S'}{D^2} \tag{10}$$

Here, the variables marked with primes are measured in the rest frame of the stellar surface [38], with $\cos\theta' = \eta\cos\theta$ and $\mathrm{d}S\cos\theta = \mathrm{d}S'\cos\theta'$. $I'(\nu',\theta')$ is the emergent radiation intensity, $\mathrm{d}S'$ is the emission area and D is the distance between the star and observer. The three Doppler factors are a result of the transformation of the intensity. An additional factor is obtained upon integration over a frequency interval considering that $\mathrm{d}\nu = (1-R_S/R)^{1/2}\eta\mathrm{d}\nu'$. Using equation (10), the time-dependent flux observed from the rotating hot spot can be determined for a given phase $\phi(t)$ (in the range 0 to 2π) using the relations between $\phi(t)$, θ and ψ in equations (1) and (2) and the appropriate emission model to compute $I'(\nu',\theta')$, which is described next.

2.2 Neutron Star Atmosphere Emission

The commonly accepted evolutionary scenario posits that MSPs acquire their rapid spins due to accretion of matter and angular momentum in a low-mass X-ray binary system [6]. Therefore, it is natural to expect MSPs to posess a substantial atmospheric layer. Due to gravitational settling, hydrogen is expected to surface within seconds and dominate the surface emission. An optically-thick hydrogen atmosphere of thickness ∼1 cm can by obtained with as little as 10^{-20} M$_\odot$ of hydrogen.

Non-magnetic hydrogen atmosphere models applicable to MSPs have been developed independently by different groups over the past 20 years [54] [42] [26] [22]. They all yield virtually identical results, with differences of only

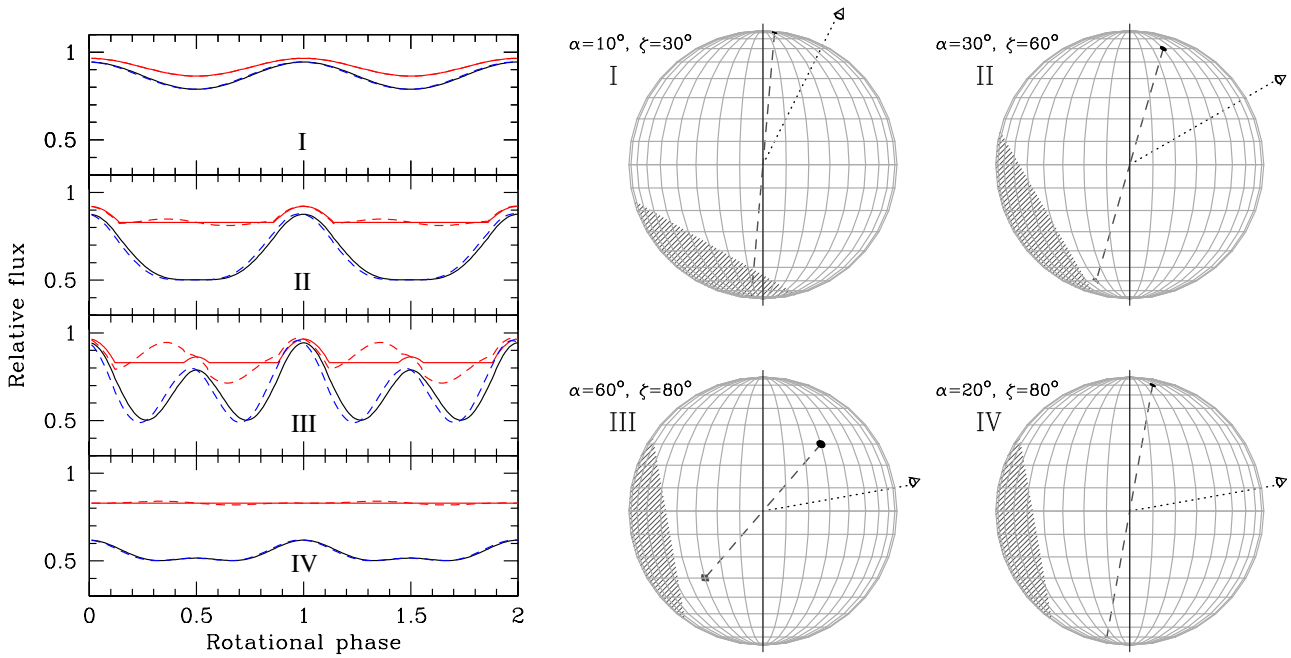

Fig. 3. (*Left*) Representative model light curves for a rotating neutron star with $M = 1.4$ M$_\odot$, $R = 10$ km and two point-like antipodal hot spots for representative geometric configurations (*right* panel). The solid curves in each plot correspond to a H atmosphere (*blue*) and isotropic blackbody emission (*red*). The dashed lines show the effects of Doppler boosting and photon travel time delays for a spin frequency of 250 Hz. (*Right*) Orthographic map projection of the NS surface for the four pulse profiles (the roman numerals I–IV correspond to the lightcurves from top to bottom, respectively). The dashed line is the axis connecting the two diametrically opposite hot spots while the dotted line is the direction to the observer. The hatched area corresponds to the portion of the star not visible to the observer. Due to gravitational bending of light, for a typical NS ∼80% of the surface is visible at any given time.

∼1% around the peaks of the emergent spectra. The models consider a static, plane-parallel atmosphere that is in radiative equilibrium, and composed of completely ionized hydrogen. As appropriate for MSPs, the surface is assumed to be weakly magnetized ($B \ll 10^{10}$ G), meaning that the effects of the magnetic field on the opacity and equation of state of the atmosphere can be safely ignored.

Relative to a standard Planck spectrum, the radiation from a neutron star atmosphere has peak emission that occurs at higher energies for the same effective temperature and exhibits an overall flux depression, which allows the conservation of bolometric flux [44] [54]. As a consequence, if modeled using a blackbody, a neutron star covered by an atmosphere would be measured to have a temperature much higher than its actual effective temperature, resulting in a grossly underestimated emitting area. Furthermore, the beaming pattern of the atmosphere is intrinsically non-uniform with radiation intensity declining as the angle with respect to the surface normal, resulting in the familiar limb-darkening effect (see Figure 2). In addition to a change in the total flux, there is a significant shift in the peak energy of the spectrum. For a blackbody spectrum no such variations are expected. This implies that although the emission spectrum is qualitatively similar to the case of a Planck spectrum, the observed shape and photon energy dependence of the rotation-induced pulsations of any localized emission on the surface (such as hot spots seen from MSPs) will differ greatly.

Using the model ingredients described above, for MSPs, synthetic pulse profiles can be generated by considering emission from two hot spots (corresponding to the two dipole magnetic polar caps) as a function of the neutron star rotational phase given a geometric configuration, temperature, emission area, and input neutron star mass and radius [11]. As seen Figure 3, the morphology of the flux modulations are determined in large part by the geometric configuration of the hot spot, neutron star spin axis and observer system. The choice of surface emission model is also a crucial factor as apparent from the substantially larger amplitude of the H atmosphere pulsations compared to a blackbody for the same assumed parameters.

It is evident from equations (2) and (10) that the measured radiation at infinity is highly sensitive to the choice of the neutron star compactness, i.e. the mass-to-radius ratio (M/R). The impact of M/R on the rotation-induced X-ray modulations of a neutron star with two diametrically opposite hot spots (corresponding to the two magnetic poles of the star) covered with a non-magnetic neutron star hydrogen atmosphere. A small increase in M/R results in a pronounced decrease in the amplitude of the pulsations (Figure 4), as a direct result of the strong dependence of the magnitude of the bending of light effect on M/R. Thus, as shown by [35] and [53], modeling of the pulsations of MSPs may can provide constraints on M and R.

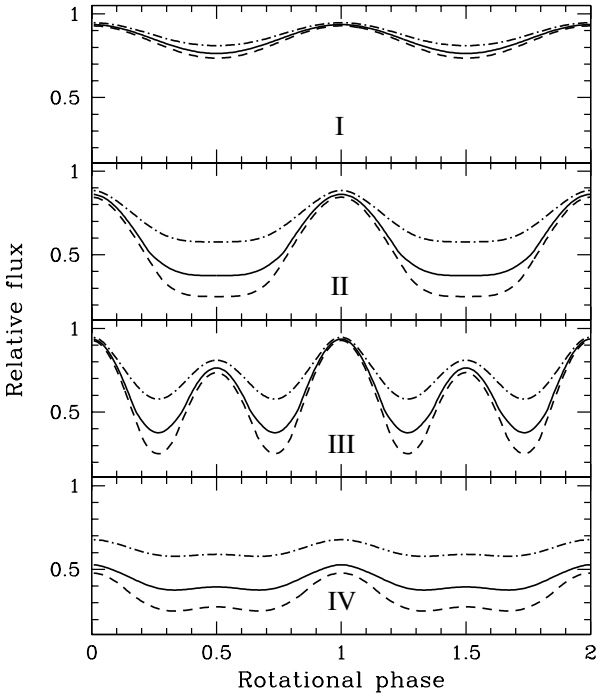

Fig. 4. Synthetic hydrogen atmosphere light curves for different stellar radii for a 1.4 $M_\odot$ neutron star star. The lines correspond to stellar radii of 9 km (*dot-dashed*), 12 km (*solid*), and 16 km (*dashed*). The angles α and ζ for each panel are assumed to have the same values as in Figure 2. Note the dramatic change in the amplitude of the rotation-induced flux variations as a function of stellar radius, caused by amplified bending of light effect for more compact stars. Two neutron star spin cycles are shown for clarity. Adapted from [11].

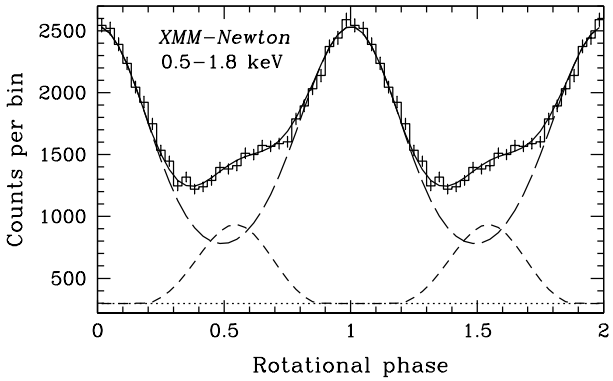

Fig. 5. The *XMM-Newton* EPIC pn pulsations of the millisecond pulsar PSR J0437–4715 in the 0.5–1.8 keV energy band with the best fit model of a rotating neutron star with two X-ray-emitting polar caps covered by a non-magnetic hydrogen atmosphere (*solid line*). The individual contributions from each hot spot are shown with the dashed lines. Note the offset from $\phi = 0.5$ of the secondary pulse, indicating a displacement of the dipole field from the center of the star. The dotted line shows the background level (see [7] for further details).

3 Observational Results

Rotation-powered MSPs were identified as pulsed X-ray sources by Becker and Trümper [4] in data from the *ROSAT* all-sky survey. The potential utillity of recycled MSPs as powerful probes of the neutron star equation of state was first pointed out by Pavlov and Zavlin [35] [53], who used *ROSAT* data of the nearest known MSP, PSR J0437–4715 [27], to demonstrate that a model of polar cap thermal emission from a neutron star hydrogen atmosphere provides a good description of the X-ray pulse profiles of this MSP, as well as to place crude limits on the mass-radius relation.

Prompted by this promising result,deep *XMM-Newton*[1] European Photon Imaging Camera (EPIC) pn observations of nearby MSPs were conducted [10] [8] [7]. These efforts confirmed that a non-magnetic hydrogen atmosphere can indeed reproduce the resulting energy-dependent X-ray pulse profiles of the two closest known MSPs, PSRs J0437–4715 and J0030+0451 (see Figures 4 and 5). In contrast, the large-amplitude pulsations are found to be incompatible with a model that considers an isotropically-emitting Planck spectrum. Furthermore, this modeling has already produced interesting constraints on the allowed neutron star equation of state (Figure 6). For PSR J0437–4715 (Figure 5), assuming 1.76 $M_\odot$ (the current measurement from radio timing [50]) the stellar radius is constrained to be $R > 11.1$ km (at 3σ confidence; Bogdanov 2013), while for PSR J0030+0451 (Figure 6) the best constraint is $R > 10.4$ (at 99.9% confidence) assuming 1.4 $M_\odot$ [8]. These limits are already inconsistent with certain quark star and kaon condensate equations of state, illustrating that this method represents a beneficial approach to probing the neutron star EoS.

Their low inferred surface magnetic fields ($\sim 10^{8-9}$ G), small emitting areas ($\leq$3 km radius), extraordinary rotational stability, and dominant and steady non-transient surface emission make MSPs fairly "clean" laboratories for studies of fundamental neutron star physics. As such, they can provide constraints on NS structure via thermal pulse shape modeling that are complementary to those derived from other approaches (e.g., using thermonuclear bursts from X-ray binaries [34] [46] [48] [39] and spectroscopy of quiescent X-ray binaries [45] [21] [25]) and thus warrant extensive studies at X-ray energies.

One advantage of using recycled MSPs is the availability of (or the possibility of obtaining) highly precise distance measurement from very long baseline interferometry (VLBI) or high-precision radio pulsar timing. The most notable example is PSR J0437–4715 for which the parallax distance has been measured to within an unprecedented $\pm 0.8\%$ (156.3 ± 1.3 parsecs) [16]. This greatly diminishes the uncertainty introduced in the emitting area, which (as seen from equation 10) is strongly covariant with the distance between the neutron star and the observer.

Perhaps more importantly, binary MSPs can offer particularly stringent constraints on the equation of state via an independent high-precision mass measurement from ra-

[1] The *X-ray Multi Mirror-Newton* is an ESA science mission with instruments and contributions directly funded by ESA Member States and NASA.

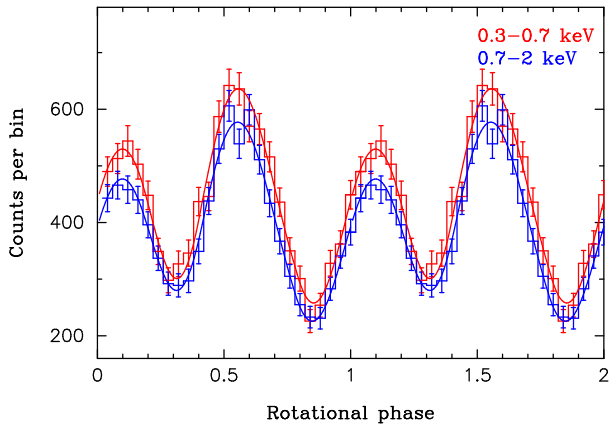

Fig. 6. The *XMM-Newton* EPIC pn pulse profiles of the nearby isolated millisecond pulsar PSR J0030+0451 in the 0.3–0.7 (red) and 0.7–2 (blue) keV ranges with the best fit model of a rapidly rotating neutron star with two H atmosphere hot polar caps [8].

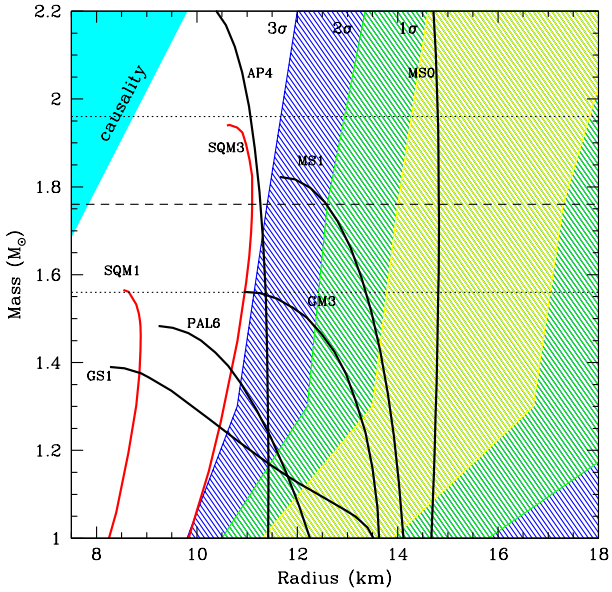

Fig. 7. The mass-radius plane for neutron stars showing the 1, 2, and 3σ confidence contours (*yellow*, *green*, and *blue* hatched regions, respectively) for the millisecond pulsar PSR J0437–4715 based on a deep *XMM-Newton* observation [7]. The solid lines are representative theoretical model tracks [28]. The horizontal lines show the pulsar mass measurement from radio timing (*dashed line*) and the associated 1σ uncertainties (*dotted lines*) [50].

dio pulse timing combined with a M/R measurement from X-ray observations. There is growing observational evidence that MSPs are systematically more massive than the canonical 1.4 $M_\odot$, as expected for neutron stars spun-up by accretion; this group includes the two most massive neutron stars known, PSRs J1614–2230 and J0348+0432 with $\approx$2 $M_\odot$ [17] [2]. This places them in an interesting region of the $M-R$ plane, away from the locus of model tracks around $R = 10$ km and $M = 1.4\,M_\odot$ (see Figure 7).

Moreover, binary MSPs permit an independent determination of the observer's viewing angle (ζ) of the neutron star since its value is expected to coincide with the measurable orbital inclination due to the expected alignment of the spin and orbital angular momentum during the accreting spin-up phase. When combined with additional geometric constraints, e.g., from modeling of *Fermi* LAT γ-ray pulsations [49], this reduces the number of free model parameters even further, thereby providing much more refined bounds on the mass-radius relation.

4 The Neutron Star Interior Composition Explorer

Existing X-ray data of MSPs are not of sufficient quality to provide meaningful constraints on neutron star structure. Nevertheless, the have served to demonstrate that MSPs can serve as astrophysical laboratories for studying ultra-dense matter. At present, further improvements in neutron star mass-radius measurements of MSPs are hindered by the design limitations of existing X-ray observatories. Their potential utility makes MSPs obvious targets for future X-ray observatories aimed at obtaining new and refining existing measurements of the $M-R$ relation [32].

Indeed, this has served as one of the principal science drivers for the Neutron Star Interior Composition ExploreR (NICER) X-ray timing instrument, currently scheduled for launch in late 2016. NICER is an approved NASA Explorer Mission of Opportunity that will be deployed as an attached experiment on the International Space Station. Its scientific payload is a non-imaging X-ray timing instrument that is composed of an array of matching 56 X-ray concentrator and silicon drift detector pairs sensitive in the 0.2–12 keV band. See Gendreau et al. [20] for a more detailed overview of the design and expected performance characteristics of NICER. Its unique combination of large effective area (nearly 2000 cm^{-2} at 1.5 keV), relatively low background, and high precision timing capabilities ($\sim$100 nanoseconds absolute time resolution) is specifically tailored for effective studies of the thermal X-ray pulsations from MSPs.

Within the nominal 18-month science mission, NICER will target the nearest recycled MSPs, PSRs J0437–4715, J0030+0451, J2124–3358 and perhaps others, in very long exposures ($\sim$1–1.5 Megaseconds), which will produce $\sim 1\times 10^6$ source photons for each target. This number of counts is sufficient to arrive at a $\sim$5% uncertainty in the measurement of the neutron star radius [41]. As demonstrated by [33], measuring the mass-radius relation of several neutron stars to better than 10% would enable very strong limits on the allowed equation of state at extreme densities [33]. Therefore, observations of MSPs with NICER hold the promise to produce a strong empirical constraint of the long sought-after pressure-density relation of cold supranuclear matter, which would have profound implications for astrophysics and nuclear physics alike.

References

1. M. A. Alpar, A. F. Cheng, M. A. Ruderman, and J. Shaham. A new class of radio pulsars. *Nature*, 300:728–730, December 1982.
2. J. Antoniadis, P. C. C. Freire, N. Wex, T. M. Tauris, R. S. Lynch, M. H. van Kerkwijk, M. Kramer, C. Bassa, V. S. Dhillon, T. Driebe, J. W. T. Hessels, V. M. Kaspi, V. I. Kondratiev, N. Langer, T. R. Marsh, M. A. McLaughlin, T. T. Pennucci, S. M. Ransom, I. H. Stairs, J. van Leeuwen, J. P. W. Verbiest, and D. G. Whelan. A Massive Pulsar in a Compact Relativistic Binary. *Science*, 340:448, April 2013.
3. M. Bauböck, E. Berti, D. Psaltis, and F. Özel. Relations between Neutron-star Parameters in the Hartle-Thorne Approximation. *ApJ*, 777:68, November 2013.
4. W. Becker and J. Trümper. Detection of pulsed X-rays from the binary millisecond pulsar J0437 - 4715. *Nature*, 365:528–530, October 1993.
5. A. M. Beloborodov. Gravitational Bending of Light Near Compact Objects. *ApJ*, 566:L85–L88, February 2002.
6. D. Bhattacharya and E. P. J. van den Heuvel. Formation and evolution of binary and millisecond radio pulsars. *PhR*, 203:1–124, 1991.
7. S. Bogdanov. The Nearest Millisecond Pulsar Revisited with XMM-Newton: Improved Mass-radius Constraints for PSR J0437-4715. *ApJ*, 762:96, January 2013.
8. S. Bogdanov and J. E. Grindlay. Deep XMM-Newton Spectroscopic and Timing Observations of the Isolated Radio Millisecond Pulsar PSR J0030+0451. *ApJ*, 703:1557–1564, October 2009.
9. S. Bogdanov, J. E. Grindlay, C. O. Heinke, F. Camilo, P. C. C. Freire, and W. Becker. Chandra X-Ray Observations of 19 Millisecond Pulsars in the Globular Cluster 47 Tucanae. *ApJ*, 646:1104–1115, August 2006.
10. S. Bogdanov, J. E. Grindlay, and G. B. Rybicki. Thermal X-Rays from Millisecond Pulsars: Constraining the Fundamental Properties of Neutron Stars. *ApJ*, 689:407–415, December 2008.
11. S. Bogdanov, G. B. Rybicki, and J. E. Grindlay. Constraints on Neutron Star Properties from X-Ray Observations of Millisecond Pulsars. *ApJ*, 670:668–676, November 2007.
12. S. Bogdanov, M. van den Berg, M. Servillat, C. O. Heinke, J. E. Grindlay, I. H. Stairs, S. M. Ransom, P. C. C. Freire, S. Bégin, and W. Becker. Chandra X-ray Observations of 12 Millisecond Pulsars in the Globular Cluster M28. *ApJ*, 730:81, April 2011.
13. T. M. Braje, R. W. Romani, and K. P. Rauch. Light Curves of Rapidly Rotating Neutron Stars. *ApJ*, 531:447–452, March 2000.
14. C. Cadeau, S. M. Morsink, D. Leahy, and S. S. Campbell. Light Curves for Rapidly Rotating Neutron Stars. *ApJ*, 654:458–469, January 2007.
15. G. B. Cook, S. L. Shapiro, and S. A. Teukolsky. Rapidly rotating neutron stars in general relativity: Realistic equations of state. *ApJ*, 424:823–845, April 1994.
16. A. T. Deller, J. P. W. Verbiest, S. J. Tingay, and M. Bailes. Extremely High Precision VLBI Astrometry of PSR J0437-4715 and Implications for Theories of Gravity. *ApJ*, 685:L67–L70, September 2008.
17. P. B. Demorest, T. Pennucci, S. M. Ransom, M. S. E. Roberts, and J. W. T. Hessels. A two-solar-mass neutron star measured using Shapiro delay. *Nature*, 467:1081–1083, October 2010.
18. L. M. Forestell, C. O. Heinke, H. N. Cohn, P. M. Lugger, G. R. Sivakoff, S. Bogdanov, A. M. Cool, and J. Anderson. A Chandra look at the X-ray faint millisecond pulsars in the globular cluster NGC 6752. *MNRAS*, 441:757–768, June 2014.
19. C. Ftaclas, M. W. Kearney, and K. Pechenick. Hot spots on neutron stars. II - The observer's sky. *ApJ*, 300:203–208, January 1986.
20. K. C. Gendreau, Z. Arzoumanian, and T. Okajima. The Neutron star Interior Composition ExploreR (NICER): an Explorer mission of opportunity for soft x-ray timing spectroscopy. In *Society of Photo-Optical Instrumentation Engineers (SPIE) Conference Series*, volume 8443 of *Society of Photo-Optical Instrumentation Engineers (SPIE) Conference Series*, page 13, September 2012.
21. S. Guillot, M. Servillat, N. A. Webb, and R. E. Rutledge. Measurement of the Radius of Neutron Stars with High Signal-to-noise Quiescent Low-mass X-Ray Binaries in Globular Clusters. *ApJ*, 772:7, July 2013.
22. C. B. Haakonsen, M. L. Turner, N. A. Tacik, and R. E. Rutledge. The McGill Planar Hydrogen Atmosphere Code (McPHAC). *ApJ*, 749:52, April 2012.
23. A. K. Harding and A. G. Muslimov. Pulsar Polar Cap Heating and Surface Thermal X-Ray Emission. II. Inverse Compton Radiation Pair Fronts. *ApJ*, 568:862–877, April 2002.
24. J. B. Hartle and K. S. Thorne. Slowly Rotating Relativistic Stars. II. Models for Neutron Stars and Supermassive Stars. *ApJ*, 153:807, September 1968.
25. C. O. Heinke, H. N. Cohn, P. M. Lugger, N. A. Webb, W. C. G. Ho, J. Anderson, S. Campana, S. Bogdanov, D. Haggard, A. M. Cool, and J. E. Grindlay. Improved mass and radius constraints for quiescent neutron stars in ω Cen and NGC 6397. *MNRAS*, 444:443–456, October 2014.
26. C. O. Heinke, G. B. Rybicki, R. Narayan, and J. E. Grindlay. A Hydrogen Atmosphere Spectral Model Applied to the Neutron Star X7 in the Globular Cluster 47 Tucanae. *ApJ*, 644:1090–1103, June 2006.
27. S. Johnston, D. R. Lorimer, P. A. Harrison, M. Bailes, A. G. Lyne, J. F. Bell, V. M. Kaspi, R. N. Manchester, N. D'Amico, and L. Nicastro. Discovery of a very bright, nearby binary millisecond pulsar. *Nature*, 361:613–615, February 1993.
28. J. M. Lattimer and M. Prakash. Neutron Star Structure and the Equation of State. *ApJ*, 550:426–442, March 2001.
29. M. C. Miller. Astrophysical Constraints on Dense Matter in Neutron Stars. *ArXiv e-prints*, November 2013.
30. M. C. Miller and F. K. Lamb. Bounds on the Compactness of Neutron Stars from Brightness Oscillations during X-Ray Bursts. *ApJ*, 499:L37–L40, May 1998.
31. S. M. Morsink, D. A. Leahy, C. Cadeau, and J. Braga. The Oblate Schwarzschild Approximation for Light Curves of Rapidly Rotating Neutron Stars. *ApJ*, 663:1244–1251, July 2007.
32. C. Motch, J. Wilms, D. Barret, W. Becker, S. Bogdanov, L. Boirin, S. Corbel, E. Cackett, S. Campana, D. de Martino, F. Haberl, J. in't Zand, M. Méndez, R. Mignani, J. Miller, M. Orio, D. Psaltis, N. Rea, J. Rodriguez, A. Rozanska, A. Schwope, A. Steiner, N. Webb, L. Zampieri, and S. Zane. The Hot and Energetic Universe: End points of stellar evolution. *ArXiv e-prints*, June 2013.

33. F. Özel, G. Baym, and T. Güver. Astrophysical measurement of the equation of state of neutron star matter. *Phys Rev D*, 82(10):101301, November 2010.
34. F. Özel and D. Psaltis. Reconstructing the neutron-star equation of state from astrophysical measurements. *Phys Rev D*, 80(10):103003, November 2009.
35. G. G. Pavlov and V. E. Zavlin. Mass-to-Radius Ratio for the Millisecond Pulsar J0437-4715. *ApJ*, 490:L91–L94, November 1997.
36. K. R. Pechenick, C. Ftaclas, and J. M. Cohen. Hot spots on neutron stars - The near-field gravitational lens. *ApJ*, 274:846–857, November 1983.
37. J. Poutanen and A. M. Beloborodov. Pulse profiles of millisecond pulsars and their Fourier amplitudes. *MNRAS*, 373:836–844, December 2006.
38. J. Poutanen and M. Gierliński. On the nature of the X-ray emission from the accreting millisecond pulsar SAX J1808.4-3658. *MNRAS*, 343:1301–1311, August 2003.
39. J. Poutanen, J. Nättilä, J. J. E. Kajava, O.-M. Latvala, D. K. Galloway, E. Kuulkers, and V. F. Suleimanov. The effect of accretion on the measurement of neutron star mass and radius in the low-mass X-ray binary 4U 1608-52. *MNRAS*, 442:3777–3790, August 2014.
40. D. Psaltis and F. Özel. Pulse Profiles from Spinning Neutron Stars in the Hartle-Thorne Approximation. *ApJ*, 792:87, September 2014.
41. D. Psaltis, F. Özel, and D. Chakrabarty. Prospects for Measuring Neutron-star Masses and Radii with X-Ray Pulse Profile Modeling. *ApJ*, 787:136, June 2014.
42. M. Rajagopal and R. W. Romani. Model Atmospheres for Low-Field Neutron Stars. *ApJ*, 461:327, April 1996.
43. H. Riffert and P. Meszaros. Gravitational light bending near neutron stars. I - Emission from columns and hot spots. *ApJ*, 325:207–217, February 1988.
44. R. W. Romani. Model atmospheres for cooling neutron stars. *ApJ*, 313:718–726, February 1987.
45. M. Servillat, C. O. Heinke, W. C. G. Ho, J. E. Grindlay, J. Hong, M. van den Berg, and S. Bogdanov. Neutron star atmosphere composition: the quiescent, low-mass X-ray binary in the globular cluster M28. *MNRAS*, 423:1556–1561, June 2012.
46. A. W. Steiner, J. M. Lattimer, and E. F. Brown. The Equation of State from Observed Masses and Radii of Neutron Stars. *ApJ*, 722:33–54, October 2010.
47. N. Stergioulas and J. L. Friedman. Comparing models of rapidly rotating relativistic stars constructed by two numerical methods. *ApJ*, 444:306–311, May 1995.
48. V. Suleimanov, J. Poutanen, M. Revnivtsev, and K. Werner. A Neutron Star Stiff Equation of State Derived from Cooling Phases of the X-Ray Burster 4U 1724-307. *ApJ*, 742:122, December 2011.
49. C. Venter, A. K. Harding, and L. Guillemot. Probing Millisecond Pulsar Emission Geometry Using Light Curves from the Fermi/Large Area Telescope. *ApJ*, 707:800–822, December 2009.
50. J. P. W. Verbiest, M. Bailes, W. van Straten, G. B. Hobbs, R. T. Edwards, R. N. Manchester, N. D. R. Bhat, J. M. Sarkissian, B. A. Jacoby, and S. R. Kulkarni. Precision Timing of PSR J0437-4715: An Accurate Pulsar Distance, a High Pulsar Mass, and a Limit on the Variation of Newton's Gravitational Constant. *ApJ*, 679:675–680, May 2008.
51. K. Viironen and J. Poutanen. Light curves and polarization of accretion- and nuclear-powered millisecond pulsars. *A&A*, 426:985–997, November 2004.
52. V. E. Zavlin. XMM-Newton Observations of Four Millisecond Pulsars. *ApJ*, 638:951–962, February 2006.
53. V. E. Zavlin and G. G. Pavlov. Soft X-rays from polar caps of the millisecond pulsar J0437-4715. *A&A*, 329:583–598, January 1998.
54. V. E. Zavlin, G. G. Pavlov, and Y. A. Shibanov. Model neutron star atmospheres with low magnetic fields. I. Atmospheres in radiative equilibrium. *A&A*, 315:141–152, November 1996.